



國立中山大學材料與光電科學學系

博士論文

Department of Materials and Optoelectronic Science

National Sun Yat-sen University

Doctorate Dissertation

矽基薄膜電晶體及氮化鎵高電子遷移率電晶體之電性

分析與物理機制研究

Investigation of Electrical Performance and Establishment of
Physical Mechanisms for Silicon-Based Thin-Film Transistors

and Gallium Nitride High Electron Mobility Transistors

研究生：孫笠荃

Li-Chuan Sun

指導教授：蔡宗鳴 博士

Dr. Tsung-Ming Tsai

中華民國 114 年 1 月

January 2025

論文審定書

國立中山大學研究生學位論文審定書

本校材料與光電科學學系博士班

研究生孫笠峯（學號：D083100008）所提論文

矽基薄膜電晶體及氮化鎵高電子遷移率電晶體之電性分析與物理機制研究

Investigation of Electrical Performance and Establishment of Physical Mechanisms for Silicon-Based Thin-Film Transistors and Gallium Nitride High Electron Mobility Transistors

於中華民國 113 年 12 月 27 日經本委員會審查並舉行口試，符合博士學位論文標準。

學位考試委員簽章：

召集人 張鼎張

委員 蔡宗鳴

委員 陳柏勳

委員 陳紀文

委員 朱哲丘

委員

委員

委員

委員

委員

指導教授(蔡宗鳴)

(簽名)

致 謝

光陰荏苒，歲月如梭，歷經十餘年的學習與研究，大學與博士研究的旅程終於接近尾聲。在此，我懷著無比感激的心情，向在此期間給予我指導、支持與鼓勵的每一位老師、同學、家人和朋友致以最誠摯的感謝。

首先，我要感謝我的指導教授張鼎張老師。從進實驗室的第一天開始，您便不遺餘力地將艱澀難懂的半導體元件物理知識與元件製程的經驗轉化為淺顯易懂的比喻，讓我快速跨過入門的門檻並順利融入實驗室。在研究資源的提供、實驗設計的調整與規劃上，您總是傾囊相授，讓我有機會能參與台積電、群創與瀚宇彩晶等公司重要的產學合作案，並從中獲得寶貴的實務經驗。您的博學、嚴謹與不懈支持讓我受益匪淺，您的專業精神和敬業態度將永遠激勵著我。

其次，我要感謝材光系的指導教授蔡宗鳴老師，感謝您在研究方向、學術討論及論文撰寫上的悉心指導，使我能順利完成博士論文。此外，我還要感謝口試委員，包括中山半導體學院的陳柏勳老師、東京威力的陳紀文部經理，以及群創光電的朱哲丘副理，感謝你們在百忙中參加我的學位考試，並閱讀我的論文提供寶貴且具體的意見，幫助我完善最終的成果。

在博士班的求學期間，我還要感謝實驗室的大家，特別是懿霆學長、志陽學長、智程學長與玉發學長。你們在研究基礎、量測分析經驗與計畫討論中給於我許多耐心的指導，對我的研究進展有著重要的影響。同時，也感謝與我同時期的同學們詠方、宇瑄、煒宸、歆妮、冠旭、宇珊、奕年與灌濡，感謝你們一路上的陪伴與鼓勵，

我們一同經歷了無數的挑戰與成長，你們是我研究期間不可或缺的重要夥伴，希望未來大家都能前途似錦、鵬程萬里。此外，我也要特別感謝實驗室的學弟妹們，包括庭慈、建宏、詠慈、娟瑋、偉傑、昱安、之稚、佳撰、泓邑、又瑄、聖堯、瑞澤、重緯、雅婷、家宏、亞寰、紘銘、裕博、涵羽、淳坤、政憲、昱霖、鈺晴、奎祐、瑞琪等，謝謝大家在實驗室研究、計畫及公共事務上用心的付出，讓實驗室充滿朝氣與活力，期許大家未來都能豐收且成功。

我要感謝材光系的諸位教授，包括黃志青教授、洪金龍教授、張六文教授、杭大任教授、周明奇教授、徐瑞鴻教授、蘇威宏教授、郭紹偉教授、蔣酉旺教授等，你們專業教導是我成長的重要基石。同時，也感謝材光系辦的顏秀芳小姐、陳秀玉小姐、張羽萱小姐等，協助我解決許多系務上的難題。此外，我還要感謝 FIB 負責人彥文學長、TEM 負責人惠君學姊、XPS 負責人施淑媖小姐、奈米核心書香姐及奈米中心惠華姐，讓我靈活擅用各種分析與製程儀器，進一步推動我的研究工作。

最後，我也特別感謝我的家人，父親孫金德先生、母親楊美惠女士的無私支持和包容，讓我在求學路上能夠專心致志，沒有後顧之憂；女友王郁雯對我的陪伴與理解，以及其一家人對我的照顧，更是我堅持下去的重要動力。感謝國防工業發展基金會對本研究項目的資助，以及國科會提供的學術資源與支持，讓我的研究得以順利推進。

博士求學的旅程雖然艱辛，但正因為有了你們的支持與幫助，我才能完成這一段難忘而有意義的旅程。再次向所有幫助過我的人致以最衷心的感謝！

孫笠峯 謹識

摘要

隨著環保需求和新興科技的快速發展，汽車產業正經歷深刻的技術變革，電動車和智能汽車的興起逐步改變了人們對車輛的定義和期望。在這一轉型過程中，車用顯示器元件和高功率元件成為重要關注對象。顯示器元件是駕駛者與車輛間的主要互動介面，不僅需精準呈現車輛的關鍵數據，如速度、能耗和導航資訊，還應滿足智能化、數字化的駕駛體驗，而高功率元件則對電動車的快充技術發揮著關鍵作用，快速充電要求元件能夠有效管理高能量輸入，縮短充電時間並提升效率，以增強電動車的日常實用性。

在顯示器元件方面，當前主流技術採用非晶矽（amorphous-Si, a-Si）或低溫多晶矽（Low-Temperature Polycrystalline Silicon, LTPS）作為薄膜電晶體（Thin-Film Transistor, TFT）的主動層材料。各種材料在成本與性能上皆有所差異，如 a-Si 具備低成本，但性能表現相對較低；而 LTPS 具備更高的電子遷移率和高性能表現，但製程成本較高。此外，可撓式顯示器技術的發展正使得聚醯亞胺（Polyimide, PI）等材料成為新興的基板選擇。這些材料不僅具備良好的熱穩定性和化學特性，還可以應用於溶液製程，實現更高的製程效率。

本論文在顯示器元件研究中，針對 TFT 提出了一種快速檢測元件品質的量測方法，解決了目前量測速度受限的問題。從元件結構和製程方面提出優化設計，確保在高溫、高濕度條件下的元件穩定運行。另外針對可撓式顯示器應用，本研究深

入分析了基於柔性聚醯亞胺基板的 TFT 物理機制，探討了其在彎折應用中的結構穩定性，為可撓式顯示器元件的商業化應用提供了理論依據和技術支持。

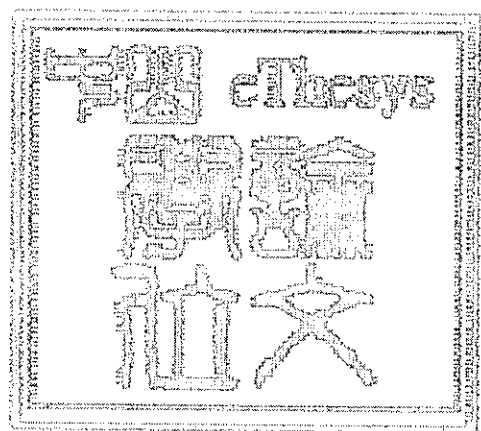
在高功率元件方面，本論文著重於氮化鎵（Gallium nitride, GaN）高電子遷移率電晶體（High electron mobility transistors, HEMTs）的性能優化。作為第三代寬能隙半導體材料之一，氮化鎵具有高擊穿電壓、高飽和電子速度以及二維電子氣的特性，使其在高功率、高頻率應用中擁有顯著優勢，被廣泛應用於功率放大器、開關器件和雷達等領域。為了進一步探索其在電動車快充中的應用，本研究針對光照對 GaN 元件性能的影響以及在不同環境壓力條件下的劣化行為進行了深入探討。

實驗結果顯示，氮化鎵元件在光照條件下會出現不同程度的性能波動，而在低氣壓環境下元件劣化速率顯著加快，這些發現為高功率元件的穩定性設計提供了依據。

此外，與碳化矽（Silicon carbide, SiC）材料相比，氮化鎵因具備更高的電子遷移率和更小的開關功率損耗，使其在高頻高功率應用中更具潛力。碳化矽雖然具有出色的高溫穩定性，但其表面散射機制的影響導致遷移率普遍偏低，限制了其在高頻應用中的發揮。

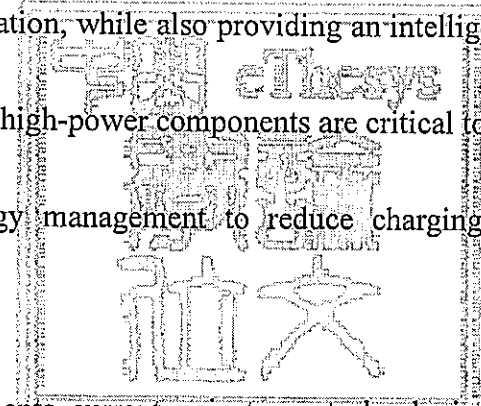
綜上所述，本論文通過對車用顯示器和高功率元件的性能優化和穩定性提升，為未來智能汽車和電動車技術的發展提供了理論支撐和技術指導。這些研究成果將在提升電動車高功率元件和車內顯示技術的應用中發揮至關重要的作用，不僅提高了駕駛體驗的數字化水平，還促進了車輛的安全性和使用便利性。

關鍵詞：車用顯示器、薄膜電晶體、高功率元件、氮化鎵、可撓式顯示器、高電子
遷移率電晶體



Abstract

The automotive industry is undergoing a profound technological transformation driven by environmental demands and the rapid development of emerging technologies. The rise of electric vehicles (EVs) and smart cars has redefined public expectations of vehicles, highlighting the importance of automotive display components and high-power components. Display components serve as the primary interface between the driver and the vehicle, requiring precision in presenting critical data such as speed, energy consumption, and navigation, while also providing an intelligent and digitalized driving experience. Meanwhile, high-power components are critical to fast-charging technology, enabling efficient energy management to reduce charging times and enhance EV practicality.



For display components, current mainstream technologies utilize amorphous silicon (a-Si) or low-temperature polycrystalline silicon (LTPS) as the active layer materials for thin-film transistors (TFTs). Each material offers unique trade-offs in terms of cost and performance, with a-Si being cost-effective but relatively low-performing, and LTPS providing higher electron mobility and superior performance at a higher production cost. Additionally, advancements in flexible display technologies have introduced polyimide (PI) as an emerging substrate material due to its excellent thermal stability, chemical resistance, and compatibility with solution-based processes.

This research proposes a rapid quality assessment method for TFTs to overcome current measurement speed limitations, introducing structural and process optimizations to ensure device stability under high-temperature and high-humidity conditions. Furthermore, it explores the physical mechanisms of TFTs on flexible PI substrates, focusing on their structural stability under bending applications. These findings offer theoretical foundations and technical support for the commercialization of flexible display components.

In the realm of high-power components, this study focuses on optimizing the performance of gallium nitride (GaN) high-electron-mobility transistors (HEMTs). As a third-generation wide-bandgap semiconductor material, GaN exhibits high breakdown voltage, high saturation electron velocity, and two-dimensional electron gas (2DEG) properties, making it advantageous for high-power and high-frequency applications such as power amplifiers, switching devices, and radar systems. This research investigates the impact of illumination on GaN device performance and its degradation behavior under various environmental stresses. Experimental results reveal performance fluctuations under illumination and accelerated degradation rates in low-pressure environments, offering insights into the stability design of high-power components.

Compared to silicon carbide (SiC), GaN demonstrates higher electron mobility and lower switching power losses, making it more suitable for high-frequency, high-power

applications. While SiC excels in high-temperature stability, its performance in high-frequency applications is limited by surface scattering mechanisms that reduce mobility.

In summary, this dissertation advances the optimization and stability of automotive display and high-power components, providing theoretical and technical support for the development of smart cars and EVs. These findings contribute to the application of high-power components and in-vehicle display technologies, enhancing driving experiences, vehicle safety, and user convenience.

Keywords: **Automotive Display, Thin-Film Transistors, High-Power Devices, Gallium Nitride, Flexible Display, High Electron Mobility Transistors**

Contents

論文審定書	i
致 謝	ii
摘 要	iv
Abstract.....	vii
Contents.....	x
Figure captions	xiv
Table captions	xxii
List of Acronyms	xxiii
Chapter 1 Introduction.....	1
1.1 Preface	1
1.2 Overview of Si-based Thin Film Transistor Technologies	5
1.2.1 Amorphous Silicon Thin Film Transistors	6
1.2.2 Low-Temperature Polycrystalline Silicon Thin Film	
Semiconductors	7
1.2.3 Typical Structures of Thin Film Transistors	8
1.3 Overview of GaN HEMT Technologies	11
1.3.1 Performance Metrics of GaN Materials	11

1.3.2	Piezoelectric Properties of GaN HEMTs.....	12
1.4	Envisioning the Future: The Evolution of Semiconductor Technology	14
1.4.1	The Development of Si-based TFTs for Outdoor Display Applications.....	14
1.4.2	Material Properties and Application Advantages of GaN HEMT	18
Chapter 2	Device Characteristics Assessment and Parameter Extractions.....	19
2.1	Transfer Characteristic Curves of Field Effect Transistors.....	21
2.2	Extraction of Threshold Voltage.....	23
2.3	Extraction of Subthreshold Slope	25
Chapter 3	Developing Rapid Testing Methods for Assessing a-Si TFTs Reliability...	26
3.1	Introduction.....	28
3.2	Fabrication of BCE Structure a-Si TFTs with Different Qualities	30
3.3	Results and Discussion	34
3.3.1	Analysis of Hysteresis Window and V_{th} Variations	35
3.3.2	Analysis of S.S. Parameters.....	37
3.3.3	Evaluating Sample Quality through S.S. Parameters	39
3.3.4	Comparison Between Positive Gate Bias Stress and Rapid Testing Methods	43
3.4	Summary.....	46

Chapter 4 Enhancing Humidity Stability of a-Si:H TFTs through High Aspect Ratio

Structure	47
4.1 Introduction.....	47
4.2 Device Fabrication.....	49
4.3 Experiment Setup.....	51
4.4 Results and Discussion	53
4.5 Summary.....	56

Chapter 5 Optimizing Bending Reliability of LTPS TFT Devices through Neutral Axis Position Control

Position Control.....	57
5.1 Introduction.....	57
5.2 Experiment.....	59
5.2.1. Degradation of Flexible Devices after Mechanical Bending	60
5.2.2. Theoretical Calculation.....	62
5.2.3. COMSOL Simulation	63
5.3 Results and Discussion	64
5.3.1 Degradation Analysis After Mechanical Bending	65
5.3.2. Theoretical Calculation of Neutral Axis Position.....	69
5.3.3. COMSOL Simulation Results	71
5.3.4. Limitations and Future Work.....	73

5.4 Summary.....	74
Chapter 6 Abnormal Hot Carrier Stress Degradation Mechanism under Vacuum Condition in AlGaN/GaN Schottky High Electron Mobility Transistor	
6.1 Introduction.....	75
6.2 Experimental Details	77
6.3 Results and Discussion	79
6.4 Summary.....	84
Chapter 7 Investigation between Recover Behavior and Defect with Variation of Light Source in AlGaN/GaN HEMTs after Hot-Carrier Stress.....	
7.1 Introduction.....	85
7.2 Experiment Setup.....	88
7.3 Results and Discussion.....	90
7.4 Summary.....	95
Conclusion.....	96
Reference.....	98
Publication.....	117

Figure captions

Chapter 1

Figure 1- 1. Comparison of radio frequency characteristics of GaN/SiC, GaN/Si, GaAs, SiGe, and Si.....	2
Figure 1- 2. GaN device strength as compared to that of Si and GaAs.....	3
Figure 1- 3. Applications of GaN materials.....	4
Figure 1- 4. A Layered Structure Diagram and the Simplified circuit of a AMLCD pixel.	
Figure 1- 5. A Cross-Section Diagram and the Simplified circuit of a AMOLED pixel..	5
Figure 1- 6. The structures of TFTs.....	8
Figure 1- 7. The schematic diagram of wurtzite GaN crystal structure.....	12
Figure 1- 8. Defective display under high temperature and high humidity quality test. (White light leakage observed in specific areas under both off mode and red light mode.).....	16
Figure 1- 9.(a) The world's first foldable smartphone will be released in 2019. (b) The horizontally stretchable screen will be developed to solve the screen crease problem.....	17

Chapter 2

Figure 2- 1. The precise semiconductor electrical measurement system used in this dissertation includes the Agilent B1500A, B2201A, and the temperature controller LakeShore 331.....	20
---	----

Figure 2- 2. The precise semiconductor electrical measurement system used in this dissertation includes the Agilent B1500A, B2201A, and the temperature controller LakeShore 331.....	20
---	----

Figure 2- 3. I_D - V_D transfer characteristic curve with different V_G values of a nMOS and pMOS.	22
---	----

Chapter 3

Figure 3- 1. Sample photograph, optical microscope image, and top-view schematic of the tested specimen.....	27
--	----

Figure 3- 2. Fabrication process flow and cross-sectional schematic of the device.....	31
--	----

Figure 3- 3. Illustration of the First H_2 Treatment.....	33
---	----

Figure 3- 4. Illustration of the Second H_2 Treatment.....	33
--	----

Figure 3- 5. Transfer characteristic curve in forward and reverse mode of the BCE a-Si TFT.....	34
---	----

Figure 3- 6. Illustration of off-state voltage operation and corresponding vertical energy	
--	--

band diagram	36
Figure 3- 7. Illustration of off-state voltage operation and corresponding transverse energy band diagram.	36
Figure 3- 8. Schematic of transverse energy band in the source barrier affected by hole injection.	36
Figure 3- 9. Diagram for reverse mode transfer curve-based top and bottom SS extraction.	38
Figure 3- 10. Comparison of bottom and top channel SS across first H ₂ treatment process variations.	40
Figure 3- 11. Excess hydrogen from the First H ₂ treatment accumulates at the GI interface and diffuses into the back channel during thermal annealing, repairing defects.....	40
Figure 3- 12. Comparison of bottom and top channel SS across second H ₂ treatment process variations.	41
Figure 3- 13. Silvaco simulation of transfer characteristics for devices with varied back-channel defect densities.....	42
Figure 3- 14. Silvaco simulation of transfer characteristics for devices with varied front-channel defect densities. variations	42
Figure 3- 15. Degradation in transfer characteristics during reliability testing under	

PBTS for samples with first H₂ treatment process variations. 44

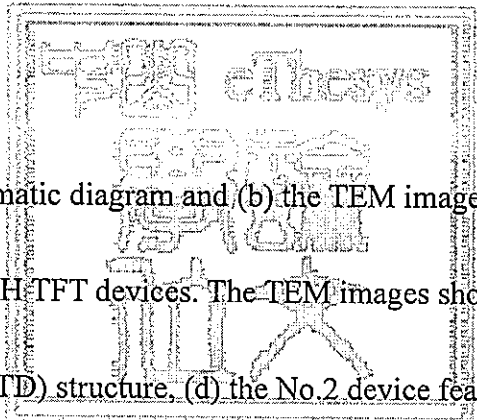
Figure 3- 16. Schematic of vertical energy band and electron trapping interface under
PBTS conditions..... 45

Figure 3- 17. Box plot of V_{th} degradation in devices with first H₂ treatment variations
after PBTS. 45

Figure 3- 18. Box plot of V_{th} degradation in devices with second H₂ treatment variations
after PBTS. 45

Chapter 4

Figure 4- 1. (a) The schematic diagram and (b) the TEM image illustrate the back-channel-etched a-Si:H TFT devices. The TEM images show (c) the No.1 device with the standard (STD) structure, (d) the No.2 device featuring a thinner channel



layer, and (e) the No.3 device with a thicker i-layer design. 50

Figure 4- 2. The transfer characteristic curves ($\log(I_D) - V_G$) for No.1 devices are
illustrated in (a) vacuum and (b) air environments. The energy band diagrams are
depicted for devices (c) without and (d) with H₂O molecules in the passivation
layer. 52

Figure 4- 3 The transfer characteristic curves ($\log(I_D) - V_G$) for the devices are shown in
an air environment: (a) No.1 (standard structure), (b) No.2 (thin channel layer), and

(c) No.3 (thick i-layer). (d) The DIBL values for devices No.1 to No.3 are presented under various relative humidity conditions..... 53

Figure 4- 4 The schematic diagrams illustrating the channel resistance distribution of a-Si:H TFT devices are shown for (a) No.1 (STD) and (b) No.3 (thick i-layer). (c)

The structure diagram created using Silvaco TCAD is presented, with the red dotted line representing the extraction line for the transverse electric field value.

(d) The distribution of the transverse electric field values is shown, with the black line representing No.1 and the red line representing No.3..... 54

Chapter 5

Figure 5- 1. The schematic structure of the LTPS TFT is presented. The test key pictures of two devices with different widths were observed under an optical microscope (OM)..... 60

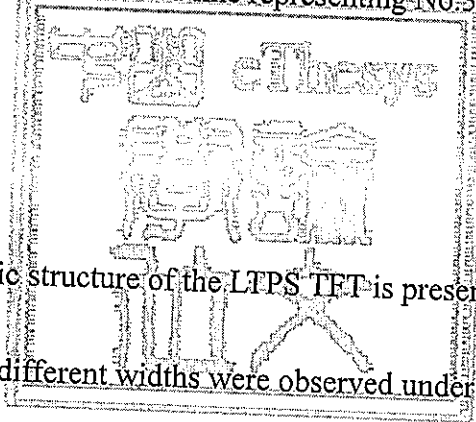


Figure 5- 2. The schematic diagram illustrates how bending tests are executed using compressive and tensile molds..... 61

Figure 5- 3. The simplified theoretical calculation of the neutral axis is provided to offer a clearer understanding of its position and behavior within the structure..... 62

Figure 5- 4. The results of the COMSOL simulation illustrate the distribution of stress

and strain across the device	63
Figure 5- 5. A two-stage trend of degradation in the threshold voltage shift (ΔV_{th}) of the I_d - V_g curve was identified, corresponding to the increase in bending time.	65
Figure 5- 6. The threshold voltage varies with bending time under compressive and tensile bending conditions in devices with channel layer widths of 5 μm and 20 μm	66
Figure 5- 7. The Silvaco TCAD simulation results verify that the generation of crack defects is a contributing factor to the first stage of V_{th} degradation.....	67
Figure 5- 8. The schematic diagram illustrates the formation of dangling bonds in the poly-Si layer resulting from long time bending.....	68
Figure 5- 9. Young's modulus of each material layer.....	68
Figure 5- 10. The influence of layer thickness and mechanical properties on the neutral axis (NA) position.	69
Figure 5- 11. A detailed view of the strain and stress distributions within the LTPS TFT structure under bending conditions is provided through COMSOL simulation....	71

Chapter 6

Figure 6- 1. (a) The device structure of a Schottky GaN HEMT and the fabrication process flow are illustrated. (b) The I_d - V_g characteristics measured at 760 torr, 1

torr, and 10^{-3} torr. (c) TLM resistance values extracted under the same pressure conditions, which are 760 torr, 1 torr, and 10^{-3} torr..... 78

Figure 6- 2. (a) Diagram of the vertical energy band structure under atmospheric and vacuum conditions. (b) Illustration of piezoelectric polarization in atmospheric pressure (760 torr) compared to vacuum (10^{-3} torr). (c) HEMT device modeled using Silvaco TCAD. (d) Current density variations corresponding to different polarization levels..... 80

Figure 6- 3. (a) I_d - V_g characteristics of the device measured in atmospheric conditions

before and after HCS. (b) I_d - V_g characteristics of the device under vacuum conditions before and after HCS. (c) Off-state drain current at different environmental pressures with $V_g = -4.5$ V. (d) Threshold voltage at various environmental pressures when $I_d = 10^{-6}$ A..... 81

Figure 6- 4. Horizontal schematics illustrating impact ionization during HCS. (b)

Vertical schematics showing the impact ionization process after HCS. (c) In atmospheric conditions, hot electrons generated by impact ionization become trapped in the AlGaN layer and GaN buffer. (d) In vacuum conditions, holes produced by impact ionization are trapped in the AlGaN layer. 83

Chapter 7

Figure 7- 1. (a) Schematic diagram illustrating the structure of the Schottky HEMT device and the materials used for its electrodes. (b) Process flow chart detailing the fabrication steps for Schottky HEMT devices. (c) Logarithmic and (d) linear Id-Vg characteristics of the devices. The transfer measurements are performed at a drain voltage (V_d) of 0.1 V. The stress conditions applied during testing are as follows:

$$V_{d,\text{stress}} = 100 \text{ V} \text{ and } V_{g,\text{stress}} = V_{\text{th,initial}} + 3 \text{ V} \text{ for a duration of 1000 seconds. 89}$$

Figure 7- 2. (a) Simulation of the electric field-distribution during HCS. (b) Schematic representation of electron trapping conditions following HCS. (c) Vertical energy band diagram of the device under HCS, showing electron injection caused by a high drain voltage..... 91

Figure 7- 3. (a) Recovery of the I_d - V_g curves after HCS in a dark environment. (b) Recovery of the I_d - V_g curves after HCS under UV light. (c) PL spectra of the AlGaN/GaN Schottky HEMT. (d) PL spectrum peaks corresponding to defect energy levels and the GaN energy gap..... 92

Figure 7- 4. (a) Changes in Ion during HCS and recovery under varying UV light intensities. (b) Ion variation during recovery under light sources with different wavelengths. (c) Vertical band diagram illustrating electron detrapping triggered by UV light after HCS..... 94

Table captions

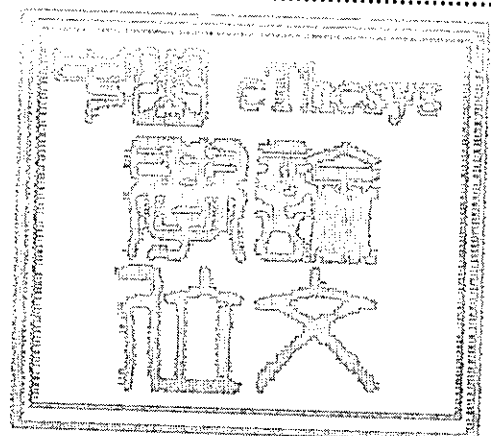
Chapter 3

Table 3- 1. Summary of Process Variations for H₂ Treatment Impact Analysis..... 32

Chapter 5

Table 5- 1. The influence of the NA due to the increase in the thickness of the buffer,

ILD, and PV layers..... 72



List of Acronyms

<i>a-Si</i>	Amorphous Silicon
<i>Poly-Si</i>	Polycrystalline Silicon
<i>TFT</i>	Thin-Film Transistor
<i>MOSFET</i>	Metal Oxide Semiconductor Field Effect Transistor
<i>HEMT</i>	High Electron Mobility Transistor
<i>G</i>	Gate
<i>S</i>	Source
<i>D</i>	Drain
<i>LCD</i>	Liquid Crystal Display
<i>OLED</i>	Organic Light Emitting Diode
<i>I_D - V_G</i>	Transfer Characteristic Curve
<i>BCE</i>	Back Channel Etching
<i>PV</i>	Passivation
<i>GI</i>	Gate Insulator
<i>ILD</i>	Inter-Layer Dielectric
<i>DUT</i>	Device under Test
<i>PECVD</i>	Plasma Enhanced Chemical Vapor Deposition
<i>SiO_x</i>	Silicon Oxide
<i>SiN_x</i>	Silicon Nitride
<i>GaN</i>	Gallium Nitride
<i>AlGaN</i>	Aluminium Gallium Nitride
<i>TEM</i>	Transmission Electron Microscopy
<i>PBTS</i>	Positive Bias Temperature Stress

